Original Article

Journal of Intelligent Material Systems and Structures

Journal of Intelligent Material Systems and Structures
2024, Vol. 35(10) 907–919

DOI: 10.1177/1045389X241241599
journals.sagepub.com/home/jim
Sage

An electromechanical impedance measurement-based solution for monitoring fresh concrete maturity

Guobiao Hu[1,2], Yaowen Yang[2], Lipi Mohanty[2], Soungho Chae[3], Kohsuke Ishizeki[3] and Lihua Tang[4]

Abstract

This paper proposes an electromechanical impedance measurement (EIM)-based solution for monitoring concrete maturity that refers to concrete strength development at the early stage. A smart aggregate (SMA) that consists of a waterproofed piezoelectric patch is developed. The working principle is explained based on the impedance theory of an electromechanically coupled system. A finite element (FE) model of the EIM-SMA unit is established. The stiffness of the applied spring foundation is varied to emulate the concrete hardening process. The simulation results reveal that a peak located between 60 and 70 kHz in the impedance plot could be used as an indication to reflect the stiffness variation of the spring foundation. A 3D-printed mold is designed for rapid production of the EIM-SMA units. In the experiment, two sample EIM-SMA units are used to monitor fresh concrete maturity in the first 6 h after casting. The results of the two sample EIM-SMA units agreed well. The experimental results matched the simulation prediction. Compared to a bar-dropping test that is widely adopted at construction sites, the impedance evolution of an EIM-SMA unit is much smoother and has better monotonicity. In general, the proposed method has been proven to be a reliable solution to monitor the maturity development of concrete.

Keywords

Concrete hydration, electromechanical impedance, piezoelectric material, structural monitoring

1. Introduction

Concrete is the most widely used material in civil engineering and construction industry over the world (Su et al. 2017). Therefore, concrete structural safety reinforcement, assessment, and evaluation have attracted lots of research attention (Bernardi et al., 2020; Dong et al., 2021; Lai et al., 2017; Qiu et al., 2021). Hydration is a complicated physical transition and chemical reaction process that strongly affects the microstructure formation in concrete materials, thus its structural strength (Stark, 2011). In civil construction, understanding the hydration process of concrete is greatly important. For instance, concrete finishing is a procedure that strives to create a smooth and durable surface. In the beginning, the concrete material is in the liquid-like phase. The concrete gradually hardens over time during the hydration process and finally transits into a solid-like phase. Thus, the finishing start time is pretty crucial (Liu et al., 2021). Improper finishing may lead to weak, flawed, and unattractive slabs (Amini et al., 2019). Construction operators have to pay close attention to concrete hardening status in the hydration process to determine the appropriate finishing start time. Monitoring concrete maturity could also help determine the optimal time to demold concrete

[1]Thrust of the Internet of Things, The Hong Kong University of Science and Technology, Guangzhou, Guangdong, China
[2]School of Civil and Environmental Engineering, Nanyang Technological University, Singapore
[3]Japan Kajima Technical Research Institute Singapore, Kajima Corporation, Singapore
[4]Department of Mechanical Engineering, University of Auckland, Auckland, New Zealand

Data Availability Statement included at the end of the article.

Corresponding authors:
Guobiao Hu, Thrust of the Internet of Things, The Hong Kong University of Science and Technology, Nansha, Guangzhou, Guangdong 511400, China.
Email: guobiaohu@hkust-gz.edu.cn

Yaowen Yang, School of Civil and Environmental Engineering, Nanyang Technological University, 50 Nanyang Avenue, Singapore 639798, Singapore.
Email: cywyang@ntu.edu.sg

components. The importance of investigating the concrete hydration process is not limited to the above cases.

According to the literature review, researchers attempted to monitor the concrete hydration process by measuring different physical parameters. It is well-known that the ultrasonic wave speed depends on the material's bulk modulus (Hauptmann et al., 1998). Since the bulk modulus of the concrete varies during the hydration process, the ultrasonic wave speed change could reflect the concrete hardening status. Based on this principle, Lee et al. (2004) proposed to monitor the hydration process by measuring the ultrasonic wave propagating speed in the concrete structure. However, a specific sample with a certain thickness has to be prepared in advance. Moreover, the instrument for measuring the ultrasonic wave speed is relatively complicated, especially for building workers without related knowledge. Therefore, this method is not suitable to be widely adopted at construction sites. Xiao and Li (2008) proposed to measure the electrical electricity of concrete through a non-contact way to determine its hydration status. The electrical resistivity evolution indicated the hydration development, and the differential provided an assessment of the rate of hydration occurring in the concrete. Since the electrical resistivity measurement apparatus is expensive and the concrete needs to be cast into a specific mold, this method is not practical for real applications at construction sites. During the hydration process, chemical transformation occurs in concrete. Different chemical composition absorbs different wavelength lights. Based on this principle, Ylmén et al. (2009) irradiated the sample concrete with infrared light with a span of different wavelengths. By the infrared spectroscopy method, the chemical composition, as well as the hydration status, could be determined. The spectroscopic signatures were correlated to the development of concrete strength. However, the authors admitted that it was very difficult to interpret the result by studying spectra only. Generally, the temperature of the concrete increases during the hydration process since the chemical reaction releases heat. Tareen et al. (2019) traced the hydration temperature history, then post-processed the data to indicate the strength change of concrete. However, this method may suffer from significant influences of the weather and environmental impact. Yang et al. (2010) designed a reusable PZT gadget to monitor the hydration process of concrete. It consisted of an aluminum enclosure attached with a PZT patch inside and two bolts tightened at the bottom. They measured the impedance of the PZT device and used the conductance as the indicator to reflect the hardening degree of the concrete structure. Their reusable gadget coupled with the concrete material through two bolts. Thus, the coupling strength was relatively weak. Moreover, after concrete mixing, they took the measurements from the third hour onwards. In other words, the early-stage information was lost. In addition, it is difficult to remove the reusable gadget from the concrete structure after complete solidification. Fan et al. (2021) designed a spherical smart aggregate for monitoring concrete hydration based on the electromechanical impedance method. Compared to a thin cylinder-like smart aggregate, the spherical one is more sensitive and can better detect the concrete status variation. They used the impedance magnitude as the indicator to reflect the concrete strength development. Talakokula et al. (2018) bonded a PZT patch to the surface of a rebar, then placed it in the concrete material. The impedance of the coupled system (PZT patch and the concrete structure) varied with the time during the hydration process. The hydration process caused an increase in the impedance. They proposed a non-dimensional parameter to indicate early-stage concrete hydration. However, the indication is insufficiently clear to capture. More relevant literature on the theme of monitoring and investigating the concrete hydration process can be found in Kim et al. (2015, 2017), Kong et al. (2013), Lu et al. (2015), Na and Baek (2018), Rao and Sasmal (2022), Rapoport et al. (2000), Su et al. (2019), and Van Den Abeele et al. (2009).

In this paper, we present an electromechanical impedance measurement (EIM) based solution for monitoring the hydration process of fresh concrete in the early times. Smart aggregates (SMA) embedded with piezoelectric materials have been developed. The fabrication procedures of the EIM-SMA units are simple, and the bare cost is pretty low. The measured impedance results of the EIM-SMA units can clearly and robustly indicate the hardening status of fresh concrete, especially at the early stage of the hydration process. In addition, the measurement can get rid of any human intervention to avoid any misoperation-caused errors.

2. Working principle

The coupling theory and the impedance method (Xu et al., 2022) are revisited in this section to explain the working principle of the proposed EIM-SMA. According to the electromechanical coupling theory, the dynamic characteristics of a piezoelectric structure are governed by the interactions between the piezoelectric element and the structure. The impedance of the piezoelectric structure is determined by the properties of the piezoelectric element, the relative location of the piezoelectric element in the structure, the boundary conditions of the structure, and the rigidity of the structure, etc. Figure 1(a) shows the schematic of a piezoelectric structure that consists of a circular-shaped PZT cylinder and a concrete cylinder. To more easily explain the dynamic interaction of the piezoelectric structure, the concrete cylinder is simplified as a lumped mass-

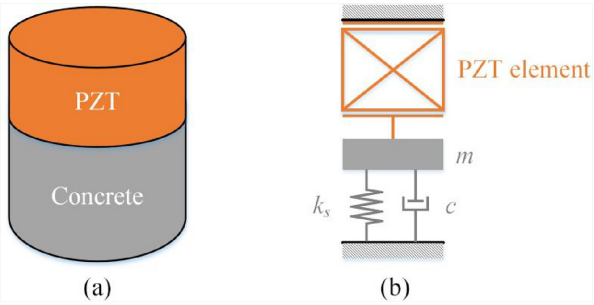

Figure 1. (a) The schematic of a circular shaped PZT patch embedded in the concrete and (b) a lumped parameter representation of the PZT-coupled concrete structure.

spring oscillator. Figure 1(b) presents the corresponding lumped parameter model. The PZT cylinder is treated as a bar with a certain piezoelectric coupling effect and elastic rigidity. For the PZT elements of the same model fabricated by a reliable manufacturer, their properties (i.e. piezoelectric coupling effect and elastic rigidity) can be assumed to be the same by ignoring the minor manufacturing errors. The concrete cylinder is simplified and represented by an SDOF mechanical oscillator with the impedance of $Z = c + im(\omega^2 - \omega_n^2)/\omega$, where $\omega_n = \sqrt{k_s/m}$, $i = \sqrt{-1}$. m, k_s, and c are the mass, spring constant, and the damping coefficient of the SDOF mechanical oscillator. The admittance (the reciprocal of impedance) of the lumped model shown in Figure 1(b) can be derived as (Liang et al., 1997):

$$Y = i\omega \frac{\pi d_A^2}{4h_A}\left(\frac{d_{32}^2 \bar{Y}_{22}^E Z_A}{Z + Z_A}\frac{\tan(kl_A)}{kl_A} + \bar{\varepsilon}_{33}^T - d_{32}^2 \bar{Y}_{22}^E\right) \quad (1)$$

where $Z_A = \frac{K_A(1+\eta i)}{\omega}\frac{kl_A}{\tan(kl_A)}i$, $K_A = \frac{Y_{22}^E \pi d_A^2}{4l_A}$, and $k = \omega\sqrt{\rho/\bar{Y}_{22}^E}$. d_A and h_A are the diameter and thickness of the piezoelectric cylinder, respectively. d_{32} is the piezoelectric constant. For the PZT material, ρ, $\bar{Y}_{22}^E$, η, and $\bar{\varepsilon}_{33}^T$ are its mass density, modulus at zero electric field, mechanical loss factor, and dielectric constant at zero stress, respectively.

After mixing cement and water, the hydration reaction takes place, resulting in shrinkage and hardening. In other words, the "stiffness" of the concrete (k_s) increases. By referring to equation (1), it is known that the concrete stiffness (k_s) change will alter the dynamic characteristics of the coupled system, which is constituted by the PZT element and the concrete material. To be more specific, as the concrete stiffness increases, the resonant frequency of the coupled system will increase as well. Therefore, it can be speculated that in the impedance plot, the resonance-related peak will shift toward the right-hand side. Based on the above principle, we propose measuring the fresh concrete impedance to monitor its maturity development.

3. Finite element simulation

In this section, a finite element model, as shown in Figure 2(a), has been developed using the commercial software COMSOL to provide a preliminary verification of the above speculation. The PZT-4 material is used to simulate the PZT element. Concrete material properties are attributed to the outside cylinder. Geometric continuity conditions are applied to the interfaces between the concrete material, the PZT material, and the copper alloy. Spring foundation boundaries are applied to emulate the surrounding environment condition (Figure 2(b)). To be more specific, the stiffness per unit length in the normal direction of the spring foundation (k_f) is described based on the designated material type (Lepillier et al., 2019):

$$k_n = \frac{E_f(1-\nu)}{d_f(1+\nu)(1-2\nu)} \quad (2)$$

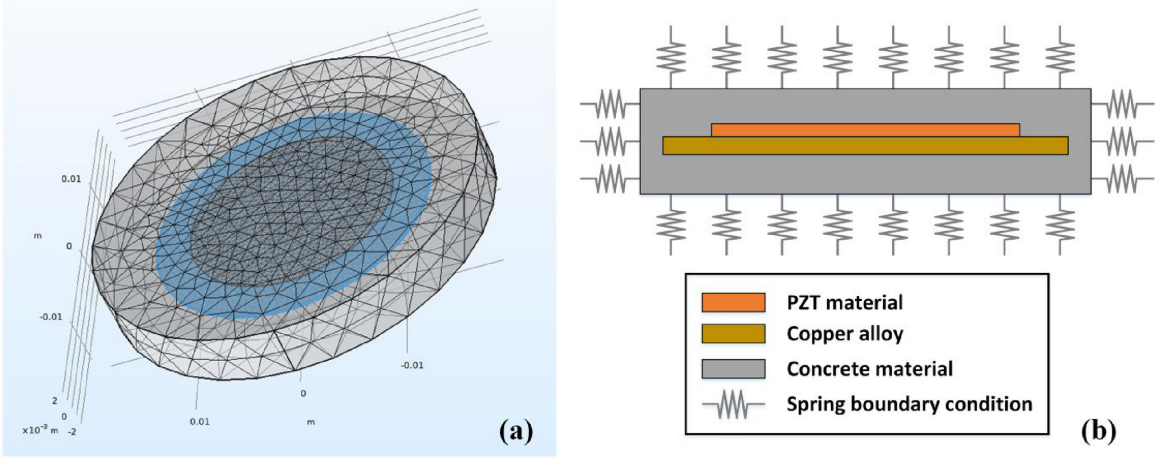

Figure 2. (a) Finite element mesh model of an EIM-SMA unit and (b) schematic of the cross-section with applied spring boundary conditions.

Table 1. Geometric and material properties of the EIM-SMA unit.

PZT patch			
PZT diameter	20 mm	PZT thickness	0.2 mm
Density	7500 kg/m^3	Young's modulus	115.4 GPa
Piezoelectric constant d_{33}	15.08 c/m^2	Relative permittivity ε_{33}	663.2
Copper alloy substrate			
Copper diameter	27 mm	Copper thickness	0.25 mm
Density	8960 kg/m^3	Young's modulus	110 GPa
Concrete substrate			
Concrete diameter	38 mm	Concrete thickness	5 mm
Density	2300 kg/m^3	Young's modulus	25 GPa

where E_f is the Young's modulus of the foundation material, ν is the Poisson's ratio, d_f is the depth of the foundation. And the shear stiffness per unit length in the tangential plane has the value:

$$k_t = \frac{E_f}{2d_f(1+\nu)} \tag{3}$$

In the simulation, we set the foundation parameters as: $d_f = 40$ cm, $\nu = 0.3$. The Young's modulus of the foundation material is varied within the range from 0.25 to 50 GPa (Jurowski and Grzeszczyk, 2015) to emulate the hardening process of the concrete.

The geometric and material properties of the EIM-SMA unit are listed in Table 1. It is worth noting that the commercial PZT wafer on the market usually consists of two layers: one layer of copper alloy substrate and another layer of PZT ceramic. Most of these parameters are consistent with the ones of the physical prototype tested in the experiment. The damping effects of these materials are described by using loss factors. The damping effect of the concrete material may vary during the hydration process and thus is difficult to describe accurately. Therefore, commonly adopted values are used in the simulation. The loss factors of the PZT material, the copper alloy, and the concrete are set to be 0.002, 0.003, and 0.04, respectively. An eigenfrequency analysis is first conducted to investigate the modal shapes of the EIM-SMA. The PZT patch is under the open-circuit condition. The first six eigenfrequencies are extracted. The modal analysis results are presented in Figure 3(a). The first three (I, II, III) and the fifth (V) modes are out-of-plane bending modes. The other two modes (IV, VI) are primarily in-plane extension modes. However, due to the geometric asymmetry of the EIM-SMA, they (IV, VI modes) are also mixed with out-of-plane bending modes. Since a thin PZT patch usually operates in the 31 mode, it can be speculated that out-of-plane bending modes can result in stronger electromechanical coupling strengths.

Subsequently, a frequency domain analysis is performed. The impedance responses of the EIM-SMA are presented in Figure 3(b). The left and right y-axes of Figure 3(b) indicate the phase and the magnitude of the impedance, respectively. It can be noted that there is one minor wrinkle around 61 kHz. The peak over the wrinkle region is formed due to the resonance of the III-mode. However, because the impedance magnitude varies over a pretty wide range, the amplitude of the small peak is inappreciable. In fact, several other peaks exist on the impedance magnitude curve in correspondence to the other resonant modes. But they are too small to be noticeable.

The resistance, that is, the real component of the impedance, is physically related to the damping/dissipative effect, thus is usually positive. Therefore, unlike the impedance magnitude that can vary over a wide range, the phase of the impedance only varies within the fixed range of $[-90°, 90°]$. For the above reason, two remarkable peaks are observed on the phase curve, as shown in Figure 3(b). The first dominant peak forms around 61 kHz, which corresponds to the eigenfrequency of the III-mode. The second prominent peak locates near 150 kHz, which corresponds to the eigenfrequency of the VI-mode. Other vibration modes induced peaks can also be detected on the phase curve. For example, one peak corresponding to the I-mode is found around 18 kHz (it is too small to observe on the impedance spectrum curve); and another peak induced by the V-mode is observed around 110 kHz. Since the III-mode induced impedance peak is the most prominent, when the condition of the surrounding foundation varies, its change can be most conveniently captured to offer a clear indication.

A parametric study is then conducted by varying the stiffness of the surrounding foundation. Since we only need to focus on capturing the change of the III-mode induced peak in the impedance plot, the frequency sweep range is limited to [50, 80] kHz. β is a dimensionless parameter to indicate the stiffness of the spring foundation.

$$\beta = \frac{E_f}{E_0} \tag{4}$$

where $E_0 = 50$ GPa, which is a typical value of the elastic modulus of concrete. Figure 4 presents the parametric study results. It can be clearly observed that

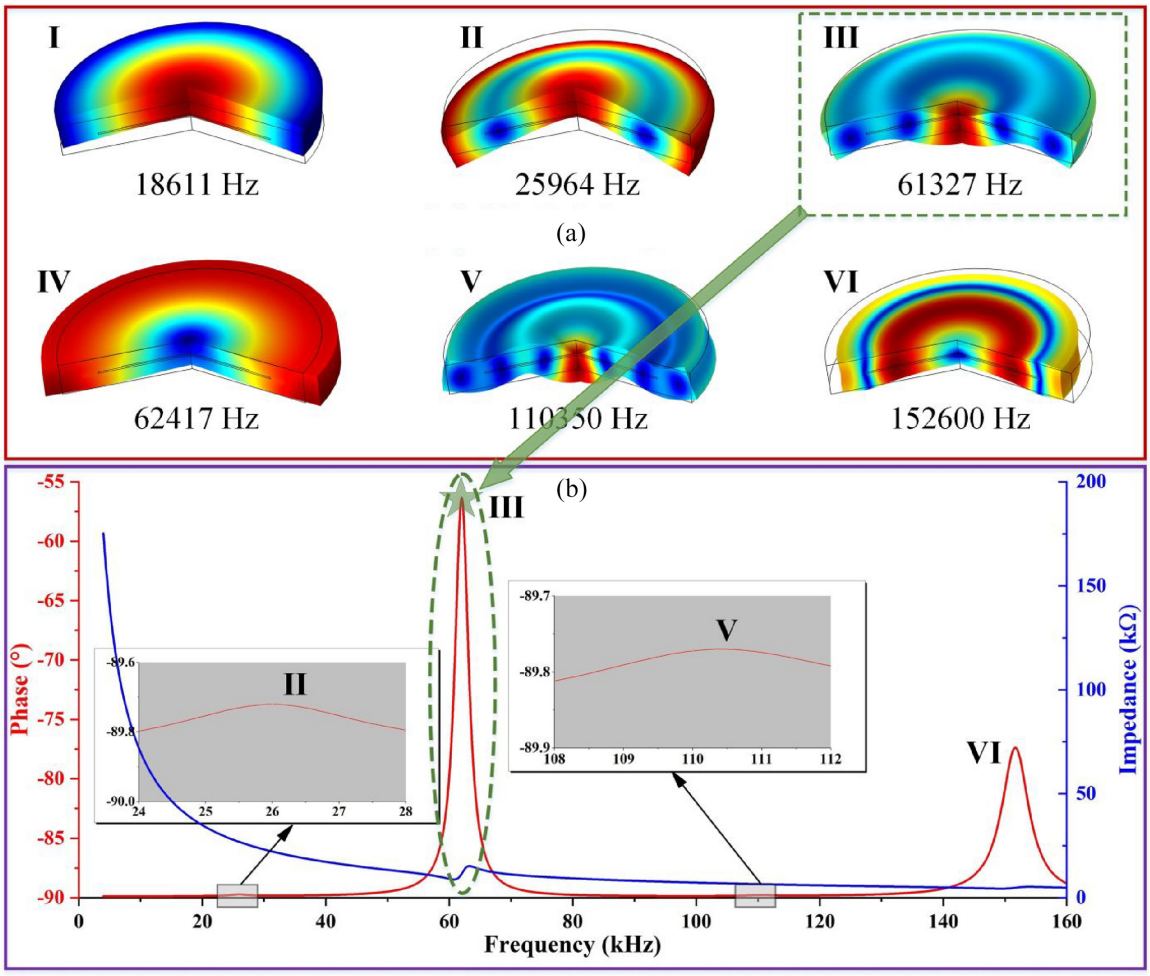

Figure 3. (a) Modal shapes of the EIM-SMA unit under spring foundation boundary conditions and (b) impedance spectrum.

with the increase of β, the peak in the impedance plot moves to the high-frequency direction. Moreover, the phase angle of the impedance decreases. The simulation results are in good agreement with our previous speculation.

4. Prototype and experimental setup

The PZT element plays the intermediary role in the proposed EIM-SMA. Because of the introduction of the PZT patch, we obtain an electromechanically coupled system that has an impedance property. Due to the coupling with the concrete material, the impedance change can reflect the concrete hardening status and provide a figure of merit to indicate the concrete maturity. In selecting the PZT patches, the ones with strong piezoelectric coupling effects are preferred to increase the sensitivity of the EIM-SMA. Moreover, the dimensions of the PZT patches are expected to be small to reduce the bare cost and miniaturize the EIM-SMA. As suitable PZT patches are selected, we have to solder the wires to the electrodes. The wires are reserved for connecting to the impedance analyzer for measurements. After soldering the wires, we have to do waterproof treatment for PZT patches before using them to make EIM-SMA. Otherwise, the two electrodes of a PZT patch will be short-circuited since fresh concrete contains water. The waterproof coating should be as thin as possible, so the piezoelectric coupling effect will not deteriorate. In the experiment, we coated the PZT

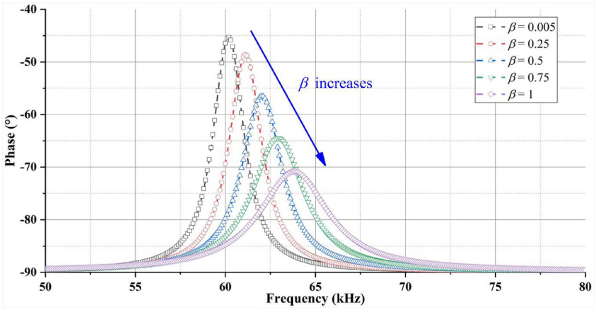

Figure 4. Impedance curves when the spring foundation stiffness (β) takes different values.

patches using insulating paints to form a thin waterproof layer.

The proposed EIM-SMA is a three-layered structure. Various methods can be employed to fabricate such three-layered EIM-SMA units. In this paper, we present a mold that is designed for the rapid production of the proposed EIM-SMA. As shown in Figure 5(a), the designed mold consists of two layers. Each layer of the mold is further divided into two components. Both the left-hand side and right-hand side components are designed with handles to ease the demolding of the EIM-SMA unit. A pair of screw holes are reserved at the edges of the two components, so they can be assembled and tightened to form a whole during the casting process of the EIM-SMA. After being independently assembled, the bottom layer forms the base with a protruded ring at the center; the top layer has a circular hole to pour in fresh concrete materials. The bottom and top layers are assembled through a sleeve connection. The EIM-SMA mold components were fabricated using acrylic 3D printers.

Figure 5(b) demonstrates the procedures of using the designed mold to cast an EIM-SMA unit. We first pour fresh concrete into the bottom layer of the mold and fill the bottom layer. Subsequently, we place the PZT patch at the center of the bottom layer and leave the wires outside of the mold. Finally, we fit the top layer on the bottom layer via sleeve connection and fill the top layer with concrete. Two sample EIM-SMA units were prepared for being used in the experiment. The concrete mix design for preparing the EIM-SMA units is as: ordinary Portland cement (OPC 425): river sand (averaged diameter < 1.18 mm): water $= 1: 0.5: 0.4$. Compared to the concrete used at construction sites, the Young's modulus of the EIM-SMA units is smaller because the averaged diameter of the fine river sands is much smaller (Beushausen and Dittmer, 2015). The concrete strength increases with larger sand particle size due to better packing and increased interlocking between the particles. When larger sand particles are used in concrete mix design, there is a more efficient packing of the particles, which reduces the amount of voids in the mixture. This denser packing leads to improved load transfer and enhanced interlocking between the particles, resulting in a higher compressive strength of the concrete. Additionally, larger sand particles can also contribute to better bonding with the cement paste, further enhancing the overall strength of the concrete. The small-sized fine river sands are used to strike a balance between the strength of the EIM-SMA units and the smoothness of the surfaces (i.e. casting accuracy).

A precision impedance analyzer 6500B from Wayne Kerr Electronics LTD is used to measure the impedance of the EIM-SMA. Its frequency sweep range is up to 120 MHz, and the impedance measurement accuracy is $\pm 0.05\%$. Measurement data can be saved as CSV files to the USB memory plugged into the USB ports on the instrument back panel. For a given EIM-SMA under the free condition, we swept the frequency from 50 to 80 kHz and noticed a distinct peak between 60 and 70 kHz, which is as expected according to the previous simulation results. An impedance is a complex number that can be expressed in terms of its real and imaginary parts. Alternatively, an impedance can be expressed in terms of its magnitude and angle. The magnitude of an impedance depends on many factors and can vary in a vast range, as well as the decomposed real and imaginary parts. During the concrete hardening process, the magnitude of the EIM-SMA's impedance may decrease quasi-monotonically. Thus, the peak corresponding to the electromechanically coupled resonance may exhibit a local maximum, which is difficult to detect. Since the natural limit of the phase angle is $[-90°, 90°]$, the peak in the phase angle plot will be more likely a global maximum. For the above reasons, in the instrument settings, we select the magnitude and angle of the impedance as the parameters to be measured.

The whole process of using EIM-SMA units to monitor concrete maturity has been graphically elucidated in Figure 6. First, we embed the fabricated EIM-SMA units into the fresh concrete at the construction site. Then, the preserved wires are connected to the

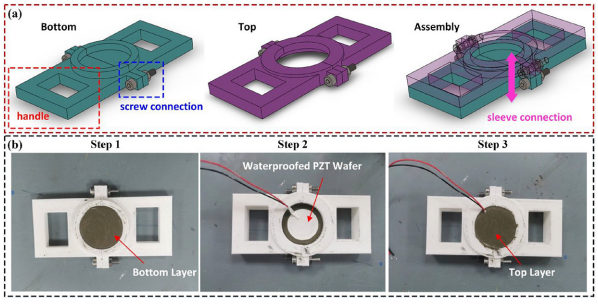

Figure 5. (a) Schematic of the mold components: bottom, top, and assembly and (b) the procedures for casting an EIM-SMA unit.

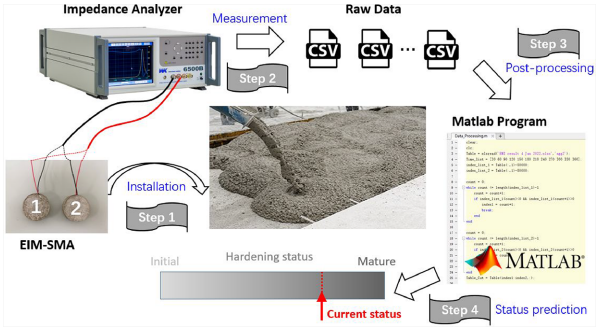

Figure 6. Procedures for using EIM-SMA units to monitor the hardening status of fresh concrete.

Table 2. Summary of mixture proportions.

Materials	Cement OPC	Cement GGBS	Water	Coarse agg	Fine agg	Admix 1	Admix 2
Mix content (kg/m^3)	400	25	170	960	815	1275	3613

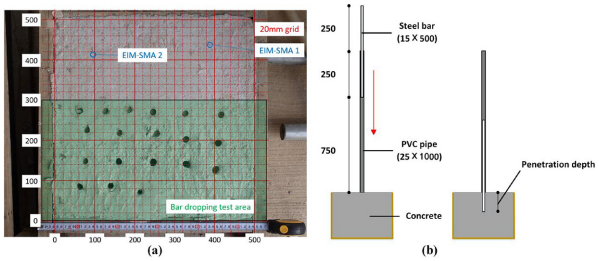

Figure 7. (a) The layout of the concrete test field. Two EIM-SMA units are embedded in the above area and the bar dropping test is conducted in the below area and (b) the bar dropping test procedure.

impedance analyzer. Subsequently, we command the impedance analyzer to make one measurement every 30 min and record the results. In the specific experiment, we measured the results in the first 6 h after concrete mixing. The measured results are collected in the raw data format and stored in the same folder. The coded MATLAB program automatically identifies the raw data, analyzes the impedance evolution, and interprets the concrete maturity development. The data processing algorithm is described in Appendix 1.

In addition to the proposed method, the conventionally widely used bar dropping test at construction sites has also been conducted in the experiment. Figure 7(a)

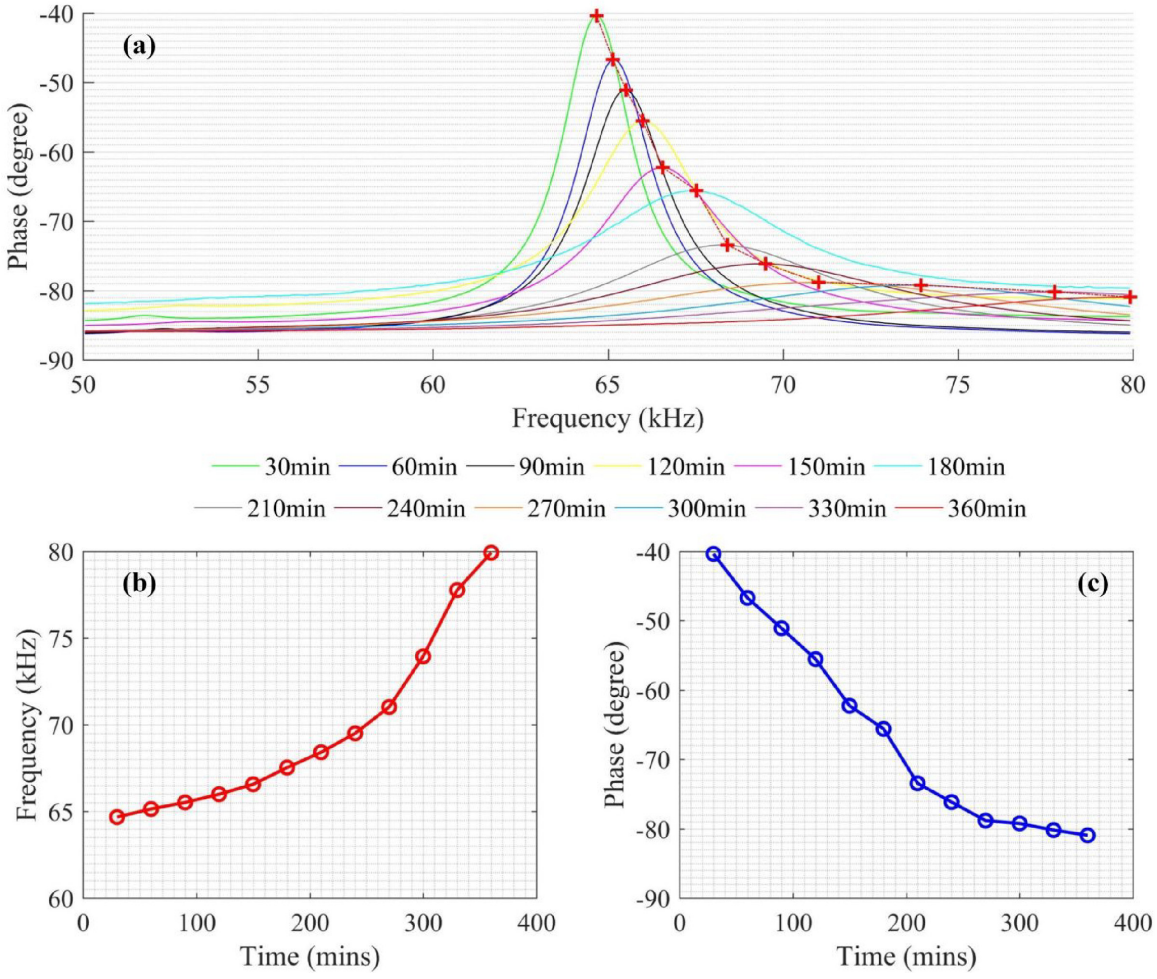

Figure 8. Impedance evolution results of sample-1 during the first 6 h after concrete mixing: (a) the overall phase curve evolution, (b) the peak frequency shift, and (c) the peak amplitude (phase) change.

shows the layout of the concrete test field. Two EIM-SMA units are embedded in the above area. The bar dropping test is conducted in the below area to avoid the influence on the impedance measurement. Figure 7(b) illustrates the bar dropping test procedure. Table 2 lists the mixture proportions of the constituent materials for the concrete to be tested and monitored in the experiment.

5. Results and discussion

The experimentally measured impedance responses of a sample EIM-SMA unit are shown in Figure 8. As predicted by the finite element simulation, we focus on capturing the change of the prominent peak that may appear between 60 and 70 kHz. The impedance responses over a wider frequency range are presented in Appendix 2. Figure 8(a) presents all the phase curves of sample-1 that were measured with a fixed time gap of 30 min. The peaks on those curves are marked with red crosses. Similar to the simulation results in Figure 4, the impedance peak moves in the high-frequency direction with time, indicating that the concrete hardens. Moreover, the peak amplitude monotonically decreases over this period. The peak-related information (frequency and phase) are extracted and separately plotted in Figure 8(b) and (c).

From the frequency shift trend shown in Figure 8(b), we can see that its increase rate is low at the beginning of the hydration process, then becomes larger in the later stage. This phenomenon agrees with the ultrasonic pulse velocity (UPV) evolution result reported in Lee et al. (2004). In the most beginning, the fresh concrete acts as a liquid-like viscous suspension for the embedded EIM-SMA unit and can barely support shear waves. In the later stage, the cement and the grains become more firmly connected, and the concrete material transforms into a solid-like phase. Therefore, the shear modulus of the concrete material increases significantly, and the concrete material behaves much stiffer. As revealed in Figure 8(c), the impedance peak amplitude (impedance phase) gradually decreases to a level that approaches −90°. Figure 8(a) shows that the peak becomes relatively flattened and challenging to

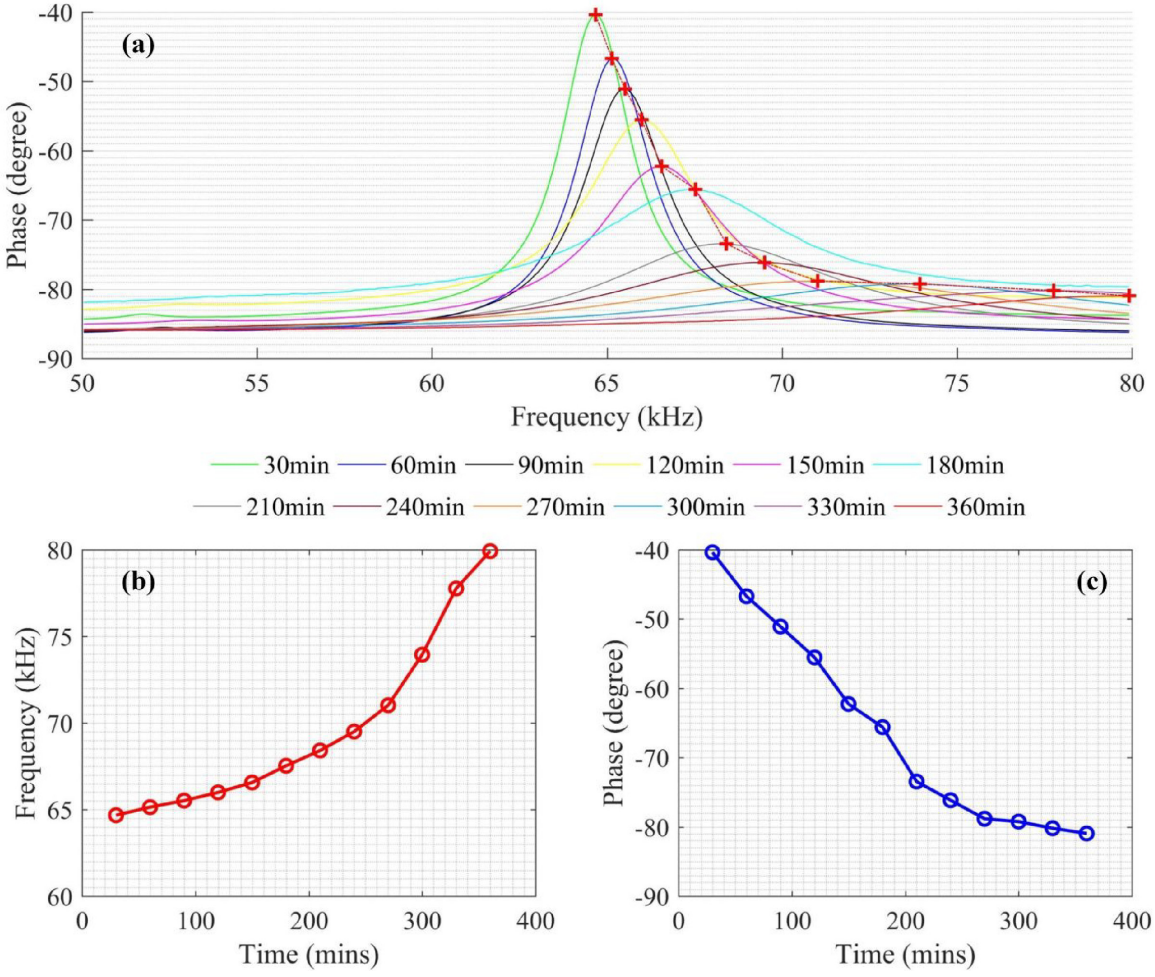

Figure 9. Impedance evolution results of sample-2 during the first 6 h after concrete mixing: (a) the overall phase curve evolution, (b) the peak frequency shift, and (c) the peak amplitude (phase) change.

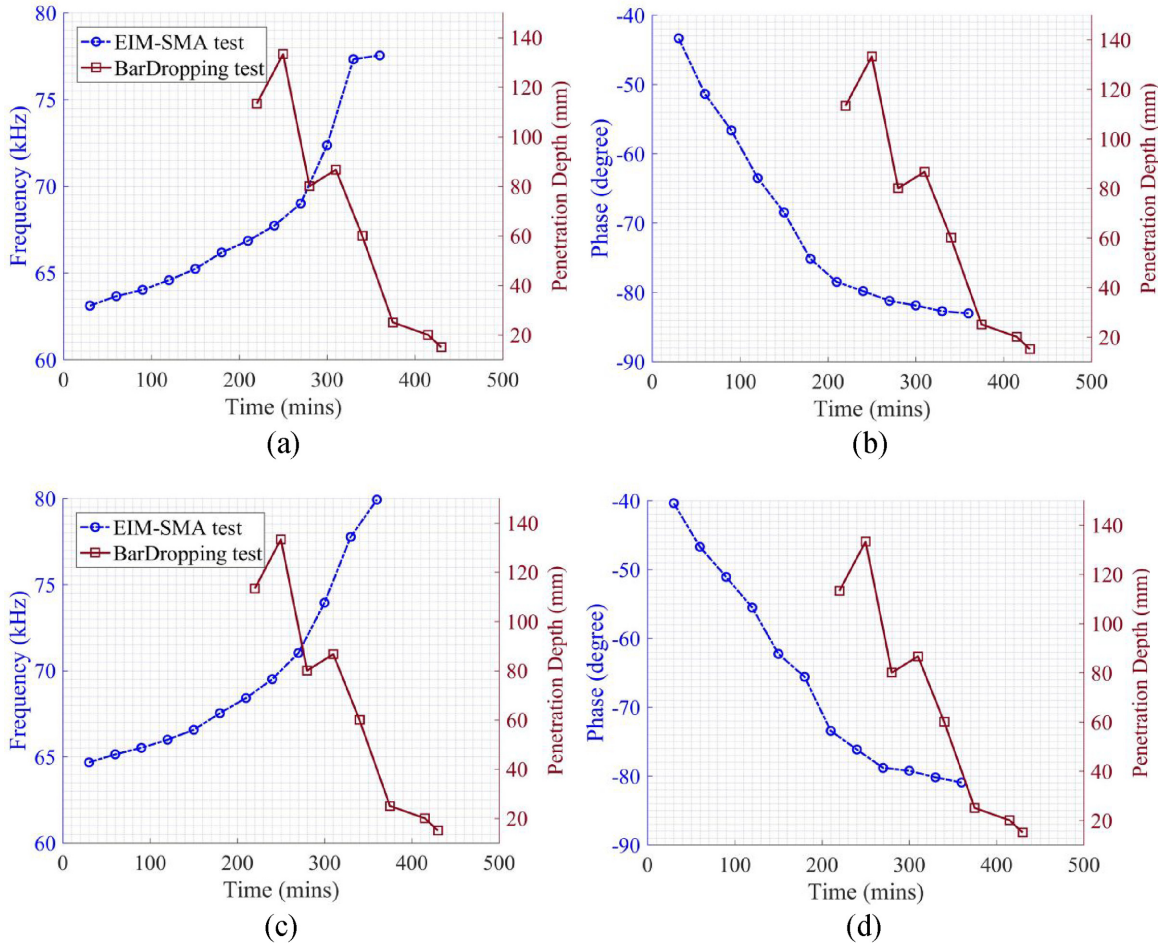

Figure 10. Correlation between the impedance results and the bar-dropping results. For sample-1: (a) peak frequencies—penetration depths and (b) phase—penetration depths. For sample-2: (c) peak frequencies—penetration depths and (d) phase—penetration depths.

capture in the later stage. From this point of view, based on detecting this indication peak between 50 and 80 kHz, this method is only suitable for monitoring the maturity development of fresh concrete in the first several hours after casting.

The experimental results of another sample EIM-SMA unit are presented in Figure 9. These two sample units were embedded in the same casting yard and tested almost simultaneously. Due to many uncertainties in the process of preparing the two sample units, their impedance responses are not exactly the same. Nonetheless, the evolution trends in Figures 8 and 9 are in good agreement: the peak moves toward a higher frequency over time, and the peak amplitude monotonically decreases. By schematizing the fabrication process more carefully, we are supposed to obtain more standardized EIM-SMA units with more consistent sensing capabilities.

In practical applications, the impedance measurement results cannot be interpreted into concrete maturity in common cognition without any reference information. Therefore, the results of a widely conducted bar-dropping test are used as the reference. It is worth noting that since the concrete material is in a liquid-like phase at the beginning, the bar penetrated through the whole thickness. Therefore, the bar-dropping test was conducted after 220 min after concrete mixing. The impedances are correlated to the bar-dropping depths to indicate concrete maturity. In order to make sure that the established correlation mapping validates for all EIM-SMA units, the EIM-SMA units have to be calibrated to exhibit the same initial impedance characteristics under the free condition, that is, before embedding into the fresh concrete. Assuming the massive production process of the EIM-SMA can be standardized, most EIM-SMA units can be exempted from calibration. In other words, a standardized EIM-SMA unit should have expected impedance characteristics.

As an example demonstration, Figure 10 shows the correlation mapping between a series of impedance results and the bar-dropping results. As the impedance

peak evolution contains both the frequency shift and phase change, Figure 10(a) and (b) illustrate the correlations of the frequencies and phase to penetration depths in the bar-dropping test, respectively. The penetration depth decreases with time as the concrete gets hardened. It can be clearly observed that the impedance peak frequency monotonically increases in this process, indicating the increase of concrete "stiffness," which echoes with the hardening of the concrete. On the other hand, the phase monotonically decreases in this process, providing another indication to reflect the concrete hardening status. To correlate the impedance results with the bar-dropping test or other reference results, we can establish a look-up table or a fitting function. Given an impedance measurement result (peak frequency and magnitude), we can interpret it into the concrete hardening status by referring to the look-up table or using the fitting function.

It is worth noting that the bar-dropping test results involve serious fluctuations: though the penetration depth overall decreases with time, it does not change monotonically. Moreover, according to practical experience, the bar-dropping test is affected by many external factors. Therefore, several in-parallel bar-dropping tests often yield non-negligibly different results. Compared to bar-dropping test results, the impedance evolution curve is much smoother and has better monotonicity. In addition, the instrument can perform impedance measurements automatically without human intervention, indicating that misoperation-caused errors can be avoided entirely in the test. Hence, the proposed approach is a more reliable solution to monitor the maturity development of concrete.

6. Conclusion

EIM-SMA units have been developed in this paper to monitor concrete maturity development in the hydration process. The working principle of the EIM-SMA units has been explained based on the impedance theory of an electromechanical coupled system. The concrete hardens over time during the hydration process, and the resonant frequency of an EIM-SMA unit that couples with the surrounding concrete increases. Thus, the peak in the impedance plot will shift to the high-frequency direction. The feasibility of the proposed method has been first verified by an FE simulation, and we have identified a peak around 60 kHz that can be used as an indicator to reflect the concrete strength development. Since the phase of the impedance varies within the fixed range of $[-90°, 90°]$, the peak on the phase curve can be remarkably observed and captured as an indication of the concrete hardening status. A 3D-printed mold has been designed for casting the EIM-SMA units. An experimental study has been conducted. The test results of the two sample EIM-SMA units are in good agreement with each other, showing the repeatability of the EIM-SMA units. The test results also matched the FE simulation predictions to a large extent. The impedance peak keeps moving in the high-frequency direction during the hydration process, indicating that the fresh concrete hardens. Moreover, the peak amplitude monotonically decreases over this period. During the initial 6 h, the proposed method can monitor the maturity development with a resolution of 30 min. To summarize, it has been proven that concrete maturity can be monitored by detecting the impedance peak frequency shift and phase decrease over time.

Declaration of conflicting interests

The author(s) declared no potential conflicts of interest with respect to the research, authorship, and/or publication of this article.

Funding

The author(s) disclosed receipt of the following financial support for the research, authorship, and/or publication of this article: This research is supported and funded by JTC Corporation. Any opinions, findings, and conclusions or recommendations expressed in this material are those of the author(s) and do not reflect the views of JTC Corporation.

ORCID iDs

Guobiao Hu https://orcid.org/0000-0002-1288-7564
Yaowen Yang https://orcid.org/0000-0002-7856-2009
Lihua Tang https://orcid.org/0000-0001-9031-4190

Data availability statement

The data that support the findings of this study are available from the corresponding authors, GH and YY, upon reasonable request.

References

Amini K, Sadati S, Ceylan H, et al. (2019) Effects of mixture proportioning, curing, and finishing on concrete surface hardness. *ACI Materials Journal* 116(2): 119–126.

Bernardi P, Michelini E, Sirico A, et al. (2020) Simulation methodology for the assessment of the structural safety of concrete tunnel linings based on CFD fire–FE thermo-mechanical analysis: A case study. *Engineering Structures* 225: 111193.

Beushausen H and Dittmer T (2015) The influence of aggregate type on the strength and elastic modulus of high strength concrete. *Construction and Building Materials* 74: 132–139.

Dong S, Wang X, Xu H, et al. (2021) Incorporating superfine stainless wires to control thermal cracking of concrete structures caused by heat of hydration. *Construction and Building Materials* 271: 121896.

Fan S, Zhao S, Kong Q, et al. (2021) An embeddable spherical smart aggregate for monitoring concrete hydration in

very early age based on electromechanical impedance method. *Journal of Intelligent Material Systems and Structures* 32(5): 537–548.

Hauptmann P, Lucklum R, Püttmer A, et al. (1998) Ultrasonic sensors for process monitoring and chemical analysis: State-of-the-art and trends. *Sensors and Actuators A: Physical* 67(1–3): 32–48.

Jurowski K and Grzeszczyk S (2015) The influence of concrete composition on Young's modulus. *Procedia Engineering* 108: 584–591.

Kim G, Kim JY, Kurtis KE, et al. (2017) Drying shrinkage in concrete assessed by nonlinear ultrasound. *Cement and Concrete Research* 92: 16–20.

Kim J, Luis R, Smith MS, et al. (2015) Concrete temperature monitoring using passive wireless surface acoustic wave sensor system. *Sensors and Actuators A: Physical* 224: 131–139.

Kong Q, Hou S, Ji Q, et al. (2013) Very early age concrete hydration characterization monitoring using piezoceramic based smart aggregates. *Smart Materials and Structures* 22(8): 085025.

Lai J, Qiu J, Fan H, et al. (2017) Structural safety assessment of existing multiarch tunnel: A case study. *Advances in Materials Science and Engineering* 2017: 1697041.

Lee H, Lee K, Kim Y, et al. (2004) Ultrasonic in-situ monitoring of setting process of high-performance concrete. *Cement and Concrete Research* 34(4): 631–640.

Lepillier B, Daniilidis A, Gholizadeh ND, et al. (2019) A fracture flow permeability and stress dependency simulation applied to multi-reservoirs, multi-production scenarios analysis. *Geothermal Energy* 7(1): 1–16.

Liang C, Sun FP and Rogers CA (1997) Coupled electromechanical analysis of adaptive material systems-determination of the actuator power consumption and system energy transfer. *Journal of Intelligent Material Systems and Structures* 8(4): 335–343.

Liu J, Lee YC and Bard J (2021) Material characterization of workability and process imaging for robotic concrete finishing. *Construction Robotics* 5(1): 73–85.

Lu Y, Ma H and Li Z (2015) Ultrasonic monitoring of the early-age hydration of mineral admixtures incorporated concrete using cement-based piezoelectric composite sensors. *Journal of Intelligent Material Systems and Structures* 26(3): 280–291.

Na WS and Baek J (2018) A review of the piezoelectric electromechanical impedance based structural health monitoring technique for engineering structures. *Sensors* 18(5): 1307.

Qiu L, Dong S, Yu X, et al. (2021) Self-sensing ultra-high performance concrete for in-situ monitoring. *Sensors and Actuators A: Physical* 331: 113049.

Rao RK and Sasmal S (2022) Electromechanical impedance-based embeddable smart composite for condition-state monitoring. *Sensors and Actuators A: Physical* 346: 113856.

Rapoport JR, Popovics JS, Kolluru SV, et al. (2000) Using ultrasound to monitor stiffening process of concrete with admixtures. *Materials Journal* 97(6): 675–683.

Stark J (2011) Recent advances in the field of cement hydration and microstructure analysis. *Cement and Concrete Research* 41(7): 666–678.

Su L, Wang YF, Mei SQ, et al. (2017) Experimental investigation on the fundamental behavior of concrete creep. *Construction and Building Materials* 152: 250–258.

Su YF, Han G, Amran A, et al. (2019) Instantaneous monitoring the early age properties of cementitious materials using PZT-based electromechanical impedance (EMI) technique. *Construction and Building Materials* 225: 340–347.

Talakokula V, Bhalla S and Gupta A (2018) Monitoring early hydration of reinforced concrete structures using structural parameters identified by piezo sensors via electromechanical impedance technique. *Mechanical Systems and Signal Processing* 99: 129–141.

Tareen N, Kim J, Kim WK, et al. (2019) Comparative analysis and strength estimation of fresh concrete based on ultrasonic wave propagation and maturity using smart temperature and PZT sensors. *Micromachines* 10(9): 559.

Van Den Abeele K, Desadeleer W, De Schutter G, et al. (2009) Active and passive monitoring of the early hydration process in concrete using linear and nonlinear acoustics. *Cement and Concrete Research* 39(5): 426–432.

Xiao L and Li Z (2008) Early-age hydration of fresh concrete monitored by non-contact electrical resistivity measurement. *Cement and Concrete Research* 38(3): 312–319.

Xu H, Wen L, Wang J, et al. (2022) Modeling and electromechanical performance of improved smart aggregates using piezoelectric stacks. *Journal of Physics D: Applied Physics* 56(5): 1–21.

Yang Y, Divsholi BS and Soh CK (2010) A reusable PZT transducer for monitoring initial hydration and structural health of concrete. *Sensors* 10(5): 5193–5208.

Ylmén R, Jäglid U, Steenari BM, et al. (2009) Early hydration and setting of Portland cement monitored by IR, SEM and Vicat techniques. *Cement and Concrete Research* 39(5): 433–439.

Appendix 1: Data processing algorithm

To monitor the maturity development of the concrete, we have to repetitively measure the impedance every 30 min. With a proper implementation of an advanced impedance analyzer, the routine measurement task can be completed by the instrument automatically and even remotely. Nonetheless, there will be many data files to process after measurement. Manually processing those data files in the CSV format is tedious and inefficient. Hence, a Matlab program is developed to automatically post-process those raw data files. Before introducing the logic of the algorithm of the Matlab program, a file naming scheme is proposed first to let the algorithm automatically identify those raw data files to be post-processed. The raw data files must be named with the same prefix, for example, agg4. A separator, such as a hyphen (-) or an underline (_), comes after the prefix. The time information should be indicated after the separator. Examples of acceptable filenames: "agg4-30mins.csv," "agg5_210mins.csv."

Figure A1 shows the flow chart of the data auto-processing algorithm. The algorithm first searches all

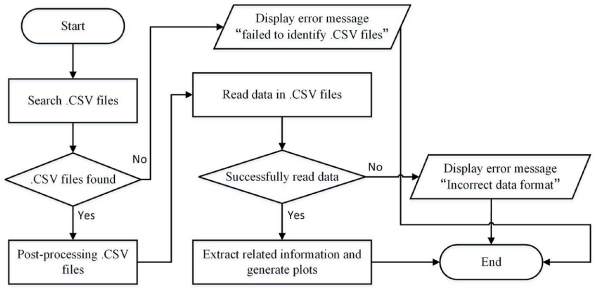

Figure A1. Flow chart of the data auto-processing algorithm.

the CSV files in the current directory. If there are no CSV files in the current directory, the algorithm will display an error message to the user. According to the prefixes and the separators that appeared in the file names, the algorithm will screen all the files first and identify the test data files. Subsequently, the data files will be sorted according to the test time information contained in the file names. The algorithm will read the data in those files by sequence. If the data files are incorrectly formatted, the algorithm will display an error message to remind the users. Assume that the data in the files are successfully read by the algorithm, they will be stored in Matlab working space. A peak search algorithm will then be used to identify the peaks and extract the corresponding frequency and phase information. Afterward, the peak evolution trend will be plotted out with respect to time to reflect the maturity development of the concrete.

Appendix 2: Impedance responses over 40–200 kHz

Figure A2 presents the experimentally measured impedance responses of the two sample EIM-SMA units. Similar to simulation results shown in Figure 3(b), the impedance response pattern is clean: only two evident peaks appear over the frequency range between 40 and 200 kHz; another minor peak is located between 110 and 120 kHz. Moreover, the peak around 60 kHz is the dominant one, which is consistent with the simulation prediction. Since the amplitude of the peak around 60 kHz is appreciably large, its change will be easy to capture. Therefore, we selected to monitor the peak at around 60 kHz to indicate concrete maturity

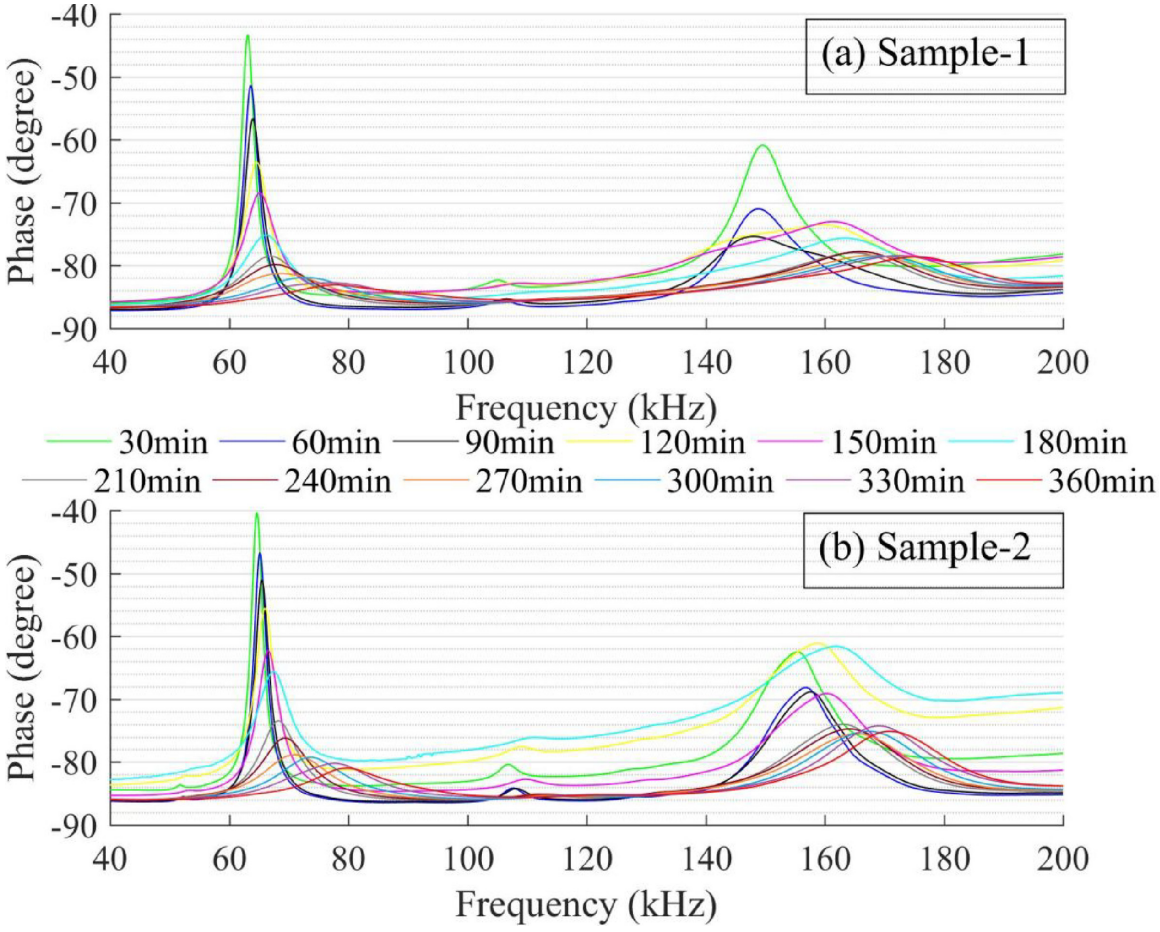

Figure A2. Experimentally measured impedance responses of the two sample EIM-SMA units over the frequency range of [40, 200] kHz: (a) sample-1 and (b) sample-2.

development. As for the two sample units, we can find that their test results are similar. The amplitude of the peak around 60 kHz decreases with the concrete curing time. Moreover, the peak location shifts toward the higher frequency direction during this process. Both features are observed in Figure A2(a) and (b). Most importantly, one can note that the variations in the two indicators can be easily detected from the beginning of the concrete curing process, which means that this technique can be applied for monitoring at the early stage of concrete strength development.